MODELLING GALVANIC CORROSION OF AEROSPACE FASTENERS AND PLATES UNDER THIN FILM CONDITIONS

Victor Kontopanos & Dr. Robert Kelly
Department of Materials Science and Engineering, University of Virginia

Abstract

Finite element modelling has been receiving increasing attention in recent years but there has not been a consensus on the best way to generate polarization data for boundary conditions for steady state modelling. To that end, the development of the activated anodic kinetic approach was undertaken to create a surface and environment undergoing active dissolution prior to the collection of the kinetic boundary conditions. Parameters were optimized for the complete activation of the aluminum alloy surface in both 0.6M and 3M NaCl and the subsequent collection of the kinetics prior to the change in the local chemical environment. These data were used in the construction of a finite element method model to be used for simulating galvanic corrosion from bulk conditions to thin film atmospheric electrolytes. Two main galvanic models were built: a single fastener set in a plate and a four-fastener plate assembly. These models were used to evaluate the effects of scribe geometry, coating on the anode, and sol gel coating of the cathode on the peak current density of SS316L and Ti-6Al-4V coupled with AA7075-T6. A framework model was constructed to be used for further assessments and has applicability to be compared to laboratory and outdoor exposures.

Introduction

Aerospace structure are generally designed using multiple material systems such as stainless steel fasteners holding together an aluminum structure. Aluminum alloys offer good strength with a low weight while also being relatively corrosion resistant and affordable. Due to the lack of weldability for many aluminum alloys, fasteners must be used. This allows for advantageous mechanical performance criteria to be met with high strength and low weight but does not optimize the corrosion performance.

There are four major requirements that must be met for galvanic corrosion to occur: anodic material, cathodic material, electrical contact, and a conductive electrolyte. The metal fasteners are generally a more noble (cathodic) material compared to aluminum alloys, such as SS316L or Ti-6Al-4V. These dissimilar material systems can cause destructive galvanic couples to form. In the presence of corrosive atmospheric electrolytes that form in the service time of the structures and components, the anodic substrate will undergo accelerated corrosion incited by the cathodic fastener material.[1] The aluminum alloy structures will often have surface treatments such as primers, topcoats, protective coatings, sacrificial pigments, paint, or other methods of masking the anodic surface area to effectively isolate the aluminum alloy from the electrolyte.[2–4] Inevitably, scratches or other imperfections will occur in the aluminum coating either from installation or through use in service; this causes bare areas of the alloy to be exposed to the electrolyte. The coupling of a small anodic surface area exposed through imperfections in the coating on the aluminum alloy substrate can lead to worse galvanic attack due to the concentration of the cathodic current on a small anodic surface area. The monitoring and maintenance required to keep aerospace structures in service and safe is quite extensive, requiring many man-hours to be spent on inspection and repairs.

Substantial experimental work has been conducted and is underway to probe galvanic corrosion and mitigation techniques. An alternative approach is to use computational methods to gain a better understanding and complement experimental work. Simulation techniques in modelling localized corrosion have been of increasing interest as they allow for swift generation of data compared to experimental testing. Computational methods can be employed for the evaluation of mitigation strategies, inception and continuation of localized corrosion, diagnosing problematic geometries or material combinations, and exploring parameter space for experimental techniques.[5–7] Finite element method (FEM) modeling is a numerical technique that solves a set of differential equations over a discretized geometry. COMSOL

Multiphysics® is an FEM software package that has been of increasing interest in recent years for modelling different types of corrosion and better understanding corrosion processes.[2,5,7–10] This software has been used for fundamental scientific studies, corrosion predictions to inform engineering specific selections, and the evaluation of mitigation strategies.[2,6,11] One of the major assets of FEM modelling is that it generally takes significant less time than experimental methods, allowing for timely assessments of many scenarios that would take much longer to complete in the laboratory.

The Laplace equation, shown in Equation 1, can be used in conjunction with experimentally determined boundary conditions to accurately solve for steady state corrosion processes while not inciting too much computational expense.[2,5,12–14]

$$\nabla^2 \Phi_l = 0 \qquad (1)$$

The Laplace equation is a partial differential equation where ∇ is the divergence and Φ_l is the electrolyte potential. In order to use this equation, one must assume that there is no bulk flow of solution through diffusional transport and that the electrolyte satisfies the electroneutrality condition.

The use of accurate boundary conditions that are representative of the situation that you are trying to model is of the utmost importance. Typically, anodic kinetics have been generated from freshly polished surfaces, but that does not necessarily reflect the state of the surface in service.[13–15] There has been a push to use alternative generation methods collecting the boundary condition data used in the model from surfaces that have already experienced corrosion.[1,8,11] To that end, some researchers have been generating kinetic data using cyclic polarization or collecting kinetic behavior after an activation step that incites corrosion on the exposed surface. There has not been much research focusing on the impact of these alternative approaches or the degree that surfaces have been activated in these methods.

The focus of this research centers on the evaluation of generating aluminum kinetics on a fully activated surface to capture the steady state dissolution as well as developing a modelling framework to simulate corrosion from thin film atmospheric electrolytes on relevant fastener / panel assemblies for aerospace applications.

Experimental Procedures

Boundary Condition Generation

Potentiodynamic polarization (PDP) curves were generated on both anodic (AA7075-T6) and cathodic materials (SS316L and Ti-6Al-4V). All electrochemical testing was conducted at ambient temperature of 25°C.

The AA7075-T6 samples were polished to 600 grit with SiC paper prior to exposure to solution with a 1 cm^2 working electrode area in 250 mL of either 0.6 M and 3M NaCl in a glass flat cell set up. The anodic PDP data were collected following the activated anodic kinetic (AAK) generation protocol, a potential versus time plot of this testing procedure is shown in Figure 1.

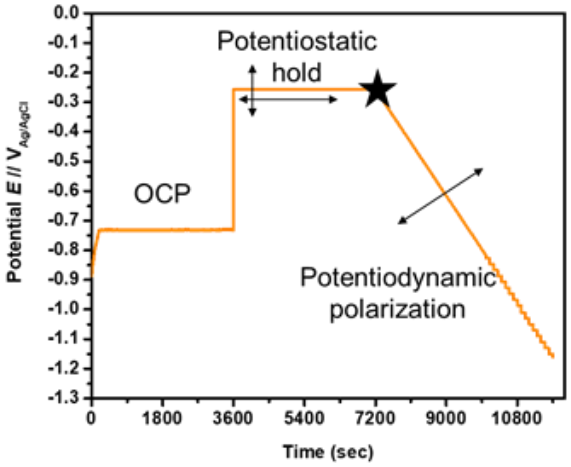

Figure 1. *Generic AAK testing protocol.*

This method follows a three-step process of 1-hr open circuit potential (OCP) followed by a potentiostatic hold, and then the kinetics acquisition with the potentiodynamic polarization. The main parameters investigated include: potential for the potentiostatic hold, time of potentiostatic hold, and scan rate during the PDP. Potentiostatic hold times ranging from 0.33 – 120 min were tested. Potentiostatic hold potentials were tested at -56, -256 and -456 mV vs Ag/AgCl reference electrode. Scan rate was varied from 0.1 – 1000 mV/s during the PDP.

Cathodic kinetic data were collected for both bare and coated SS316L and Ti-6Al-4V with a 1 cm^2 exposed surface area in 0.6M NaCl. Samples were polished to 1200 grit with SiC paper.

The rotating disc electrode (RDE) method was used to generate kinetic data for SS316L over a range of water layer thicknesses, 16µm up to bulk

(1000+ µm), by altering the rotation rate. Testing was conducted in 600 mL of either 0.6M or 3M NaCl solutions. The exposed disc was 5 mm in diameter and shrouded in Teflon. A 1-hr OCP was held prior to the collection of the PDP curves. Scan rates for all cathodic PDP was 0.2 mV/s and begun at 20 mV above OCP scanning down to -1.5 V vs. Ag/AgCl.

Finite Element Method Modelling

Version 6.0 of the COMSOL Multiphysics© FEM modelling software was used with a secondary current distribution. Several geometries were constructed with the incorporation of experimentally determined boundary conditions previously described to act at the kinetic behavior of the different solution metal interfaces from the model assembly. Several important assumptions were made:

1. Steady state conditions were assumed to be in effect over the system. This allowed for the use of the Laplace equation in the simulations.
2. The solution water layer was conformal to the assembly.
3. Migration was assumed to be the dominating means of mass transport while diffusion and convection were ignored.
4. Any coating on the aluminum substrate was assumed to be perfectly insulating and there was no undercutting of the coating by the solution.

Two main geometric models were used in this work: a single fastener set into a plate, and a four-fastener plate assembly. The single and multiple fastener assemblies allow for simulating more realistic corrosion damage and location relative to parts used in aerospace structures and can be used for evaluating mitigation strategies, different geometric considerations, etc. The effects of three different fastener head geometries were studied in this work including: hexagonal, rivet, and countersunk fastener heads, Figure 2. These single fastener head geometries were used to simulate galvanic corrosion from two different couples and the potential mitigation of this corrosion from the use of a barrier coating applied to the cathodes.

Fasteners are never used in isolation but rather there are generally going to be many together in a real aerospace assembly. A four-fastener geometry was built in the FEM software to better understand the potential risk of multiple fasteners coupling together and potentially harmful synergies, Figure 3.

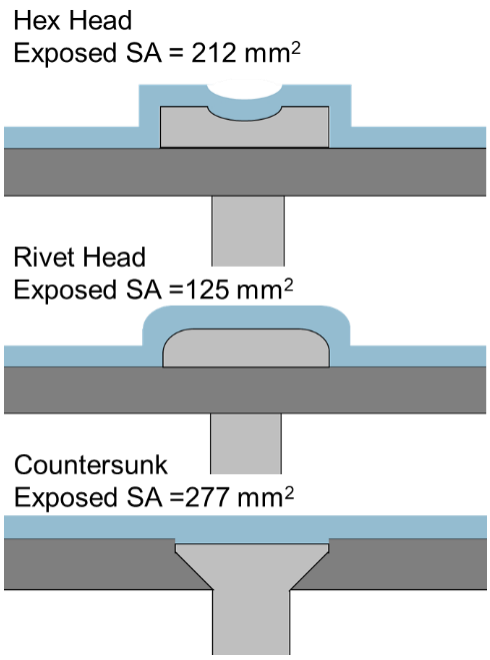

Figure 2. *Three different fastener geometries with their respective exposed cathodic surface areas and conformal water layers.*

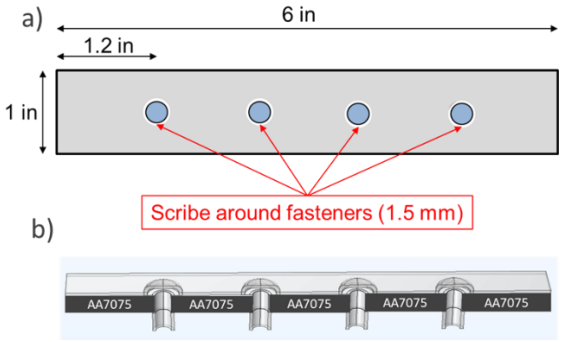

Figure 3. *a) top view schematic of the four-fastener assembly to show spacing and scribing b) side view of the water layer built around the assembly in COMSOL Multiphysics©.*

Results & Discussion

Activated Anodic Kinetics

In order to evaluate the effect that scan rate has during PDP on activated anodic surfaces, the rate was varied from 0.1 – 1000 mV/s following anodic surface activation at -256 $mV_{Ag/AgCl}$ for 60 min in 3M NaCl for a consistent surface while

studying the effect of scan rate. Figure 4 shows how the PDP curves change with increasing scan rate.

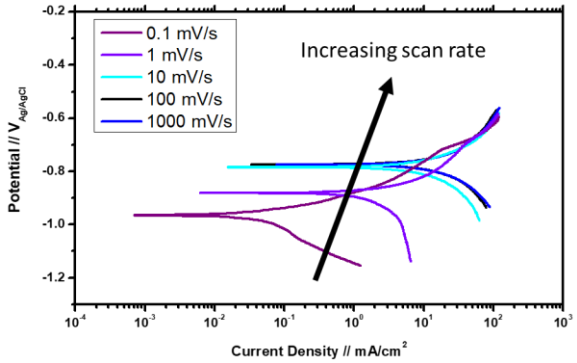

Figure 4. *AAK data collected after 60 min potentiostatic hold at -0.256V vs. Ag/AgCl in 3M NaCl with dE/dt = 0.1-1000 mV/s. Curves have been IR corrected.*

As scan rate is increased, there is an increase in the corrosion current density and corrosion potential. This can be explained by the cathodic kinetics accelerating while the anodic kinetic sides of the PDP curve appear to be converging toward the same line. The increasing cathodic kinetics are attributed to the increasing amount of Al^{3+} ions in solution generated during the anodic potentiostatic hold.[16] As scan rate increases, the time for diffusion of these species away from the surface decreases. This retention of Al^{3+} and local acidic pH (due to Al^{3+} hydrolysis) cause a more aggressive local chemistry at the surface of the sample.

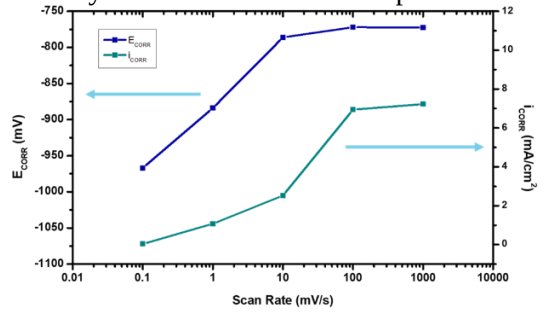

Figure 5. *Corrosion potential and current density versus time for AAK data shown in Figure 4.*

From Figure 5 it can be concluded that the kinetics are independent of the scan rate above threshold of 100 mV/s. Above this scan rate, there is not enough time to allow for any diffusion of species in solution away from the metal-solution interface. For scan rates above 100 mV/s, the solution chemistry is in essence frozen for the duration of the PDP acquisition.

The effect of the hold time for the potentiostatic conditioning step on the PDP curves is plotted in Figure 6. A fast scan rate of 100mV/s was selected for this study to maintain constant chemistry at the surface of the sample at the conclusion of the potentiostatic step and through the PDP curve acquisition.

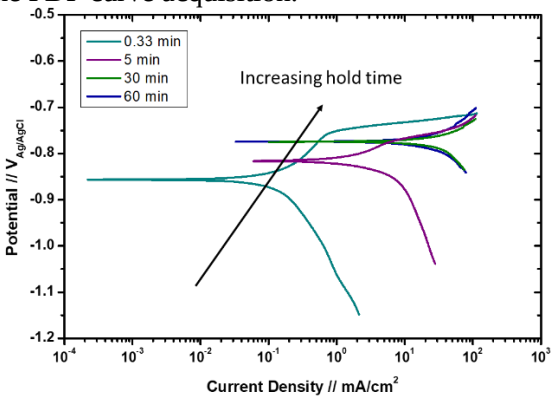

Figure 6. *AAK data collected after 0.33-60 min potentiostatic hold at -0.256V vs. Ag/AgCl in 3M NaCl with dE/dt = 100 mV/s. Curves have been IR corrected.*

A similar trend compared to the scan rate effect can be observed where the anodic kinetic branches are all approaching the same line, but that there are significant changes in the measured cathodic kinetics as the duration of the potentiostatic step is increased. This follows the same logic as the rationale for the increase in cathodic kinetics with scan rate. The longer potentiostatic hold will generate more Al^{3+} in solution that will be retained proximate to the surface during the PDP due to the fast scan rate.

After a 30-min potentiostatic hold, there is not significant change or increase in the degree of activation based on the electrochemical data. This is confirmed by the scanning electron microscopy (SEM) image shown in Figure 7 that indicates that the localized corrosion has spread across the entirety of the exposed surface area. Pitting corrosion that initially began from micro galvanic couples and crystallographic attack progressed and converged such that the surface became fully activated.

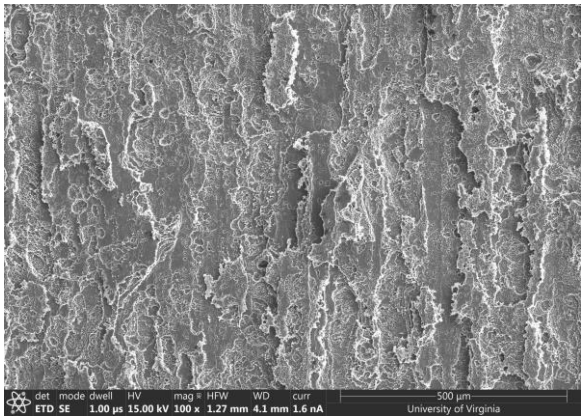

Figure 7. *100x SEM image of surface morphology from surface activation in 3M NaCl.*

It was confirmed that the AA7075-T6 surface will undergo complete activation with a 30 min potentiostatic hold at -256 $mV_{Ag/AgCl}$ in 3M NaCl. The parameters optimized for 3M NaCl solution are not necessarily the same for 0.6M NaCl solution, which is often used to substitute for ocean water in corrosion laboratory testing. Using the optimized scan rate of 100 mV/s for the AAK, the hold time necessary for full activation of AA7075-T6 in 0.6M NaCl was determined. Figure 8 shows the affect that increasing the duration of the potentiostatic hold has on AA7075-T6 PDP curves and representative surface morphologies associated with each.

It can be observed that the anodic kinetic branches from these PDS curves are converging onto the same line while the cathodic kinetics are increasing (i.e., exhibiting higher current densities at the same potential). This effect causes a slight shift upward for the OCP. Additionally, as seen previously through the analogous scan rate study previously reported, the increasing hold time causes increased dissolution of the aluminum into solution and accelerated cathodic kinetics. After 90-min surface activation hold, the surface morphologies and related kinetics are virtually identical. It is concluded that a potentiostatic hold at -0.256V vs. Ag/AgCl of 90 min in 0.6M will yield a fully activated surface. Additional hold time above 90 min will not change the kinetics as the surface has been fully activated.

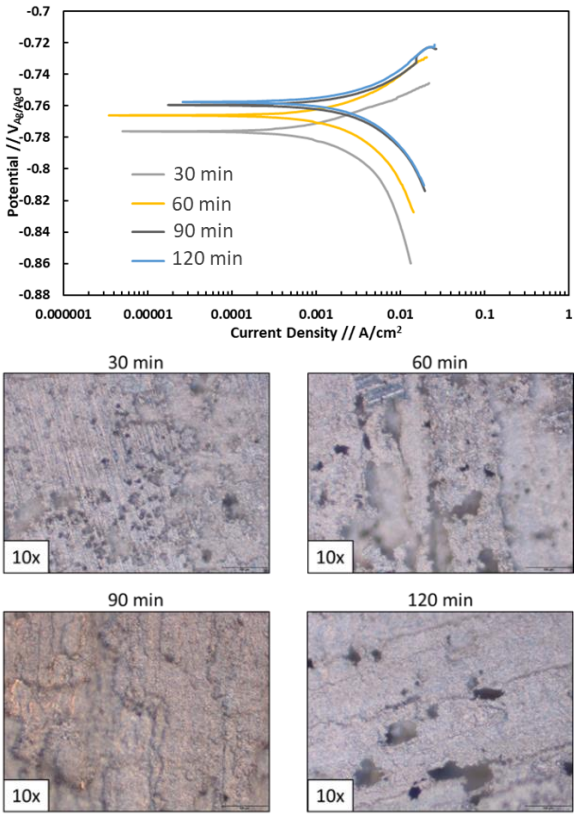

Figure 8. *AAK data collected after variable potentiostatic hold times (30-120 min) at -0.256V vs. Ag/AgCl in 0.6M NaCl with dE/dt = 100 mV/s. Curves have been IR corrected. Optical images of AA7075-T6 surfaces after potentiostatic hold at -256mV vs. Ag/AgCl for variable times in 0.6M NaCl.*

FEM Modelling Results

Figures 9 and 10 show the polarization curves used for the cathodic kinetics needed for the fasteners in the model. The anodic kinetics used in the model were shown in Figures 4 and 8; the AAK of AA7075-T6 after 60 min activation in 3M NaCl and after 120 min activation in 0.6M NaCl both collected with scan rates of 100 mV/s.

The barrier coating applied to SS316L and Ti-6Al-4V greatly reduced their cathodic kinetics, knocking the current densities down by about two orders of magnitude compared to the bare materials. FEM fastener models will be used to better understand the impact that this barrier coating has as a potential mitigation strategy for galvanic corrosion.

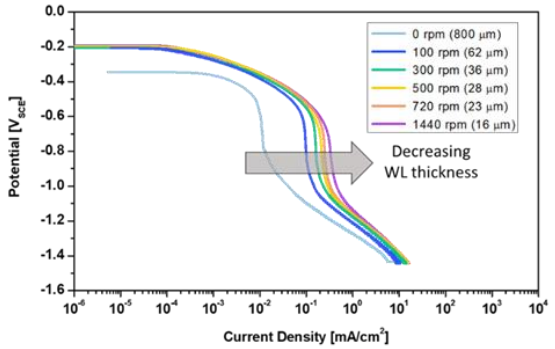

Figure 9. *Cathodic kinetics of SS316L collected with the RDE in 3M NaCl.*

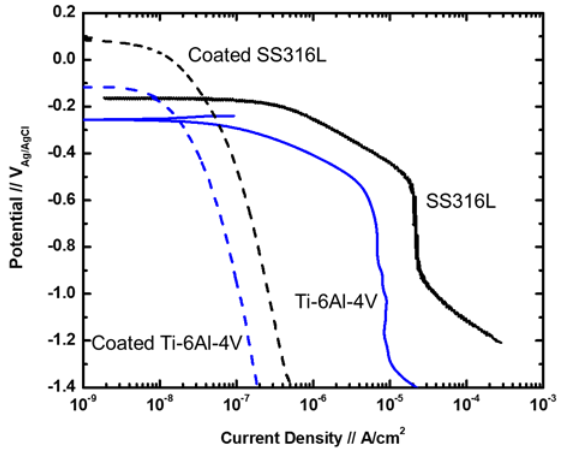

Figure 10. *Cathodic kinetics gathered in 0.6M NaCl on bare and coated SS316L and Ti-6Al-4V.*

Several different modelling scenarios were developed for screening galvanic corrosion issues that may arise in service of the aerospace industry. First, the impact of coating the anode was evaluated. Simulations were conducted with a bare fastener set in bare AA7075-T6 and coated but scribed AA7075-T6 substrate exposed to 0.6M NaCl, Figure 11. This showed that there is a significant disadvantage to coating anodic material arising from imperfections in the coating that arise from installation, service, or repair and represented by the surrogate ring scribe around the fastener head. The coated by scribed AA7075-T6 has significantly higher, approximately 30x, current densities compared to the bare substrate due to the reduction of the anodic surface area. The same trend from the rivet head geometry was observed for the hexagonal and countersunk fastener head simulations as seen in chart from Figure 12.

The metric of peak current density will be used to compare the projected severity of corrosion damage from the FEM simulations.

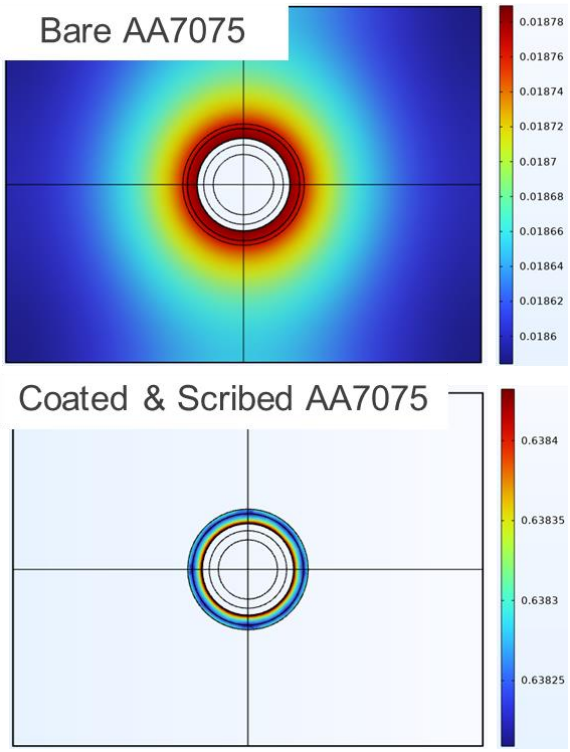

Figure 11. *Current density false color plots of bare as well as coated + scribed AA7075 substrate coupled with SS316L for the rivet head geometry.*

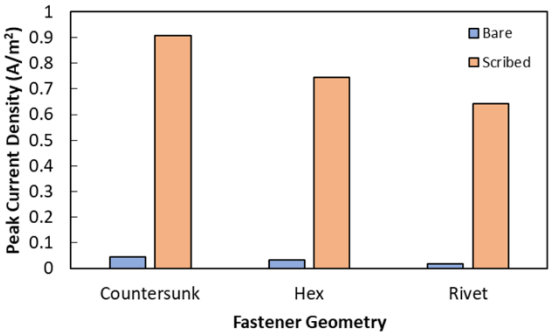

Figure 12. *Peak current density for bare and coated + scribed AA7075 coupled with bare SS316L in a 1000 µm WL of 0.6M NaCl.*

The hierarchy of the peak current density: countersunk, hexagonal, and rivet fastener heads follow the same order as the exposed cathodic surface areas.

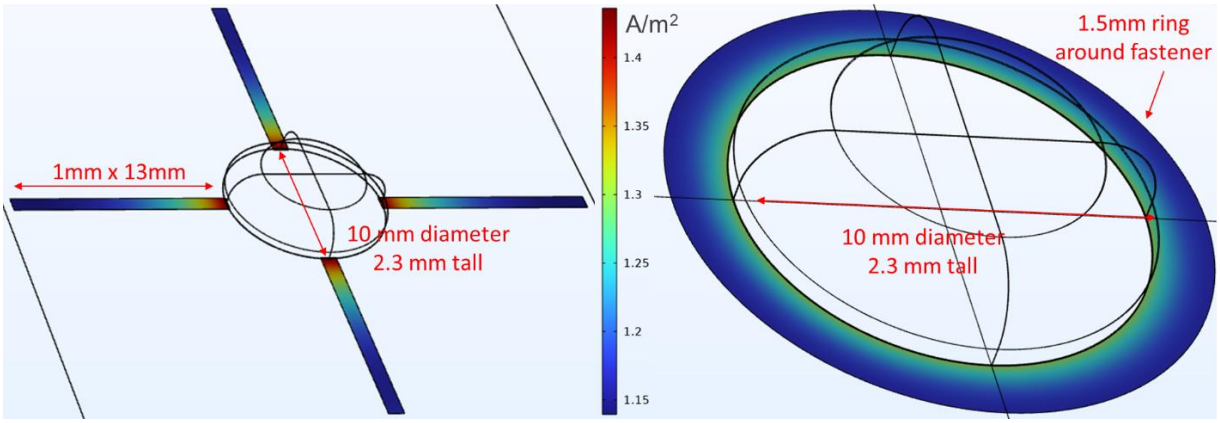

Figure 13. *Cross and circle scribe geometries with current density distributions normalized to the same color scale.*

The rivet fastener head model was used to determine the impact that the geometry of the scribe on the coated aluminum substrate has on the peak current density. Simulations were conducted in 3M NaCl for a range of water layers from 20 – 1000 µm.

A typical cross scribe centered on the fastener was compared to a ring scribe circling around the fastener head. The current density distributions for the 20 µm WL exposure simulation for the two scribe geometries are shown in Figure 13; the color scale is normalized across the two for direct comparison of the peak current densities. The exposed anodic surface area is equal in both geometries.

The smaller surface area directly proximate to the fastener on the cross scribe leads to a slightly higher peak current density (5%) compared to the ring scribe. This impact is small, leading to the assertion that the shape of the scribe will not significantly affect the maximum potential corrosion damage for continuous water layers. This may break down as water layer decreases such that it forms a discontinuous / droplet film coverage. Figure 14 shows a decreasing impact of the geometric effect as the water layer increases to the bulk exposure condition of 1000 µm.

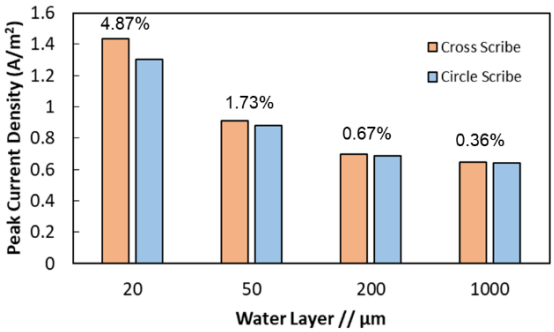

Figure 14. *Effects of the scribe geometry across a range of water layers from 20-1000 µm determined by the peak current densities predicted.*

Comparing the peak current densities from the three single fastener head geometries for both the SS316L and Ti-6Al-4V galvanic couples allows for a direct comparison of the associated corrosion risk. FEM simulations were conducted in 0.6M NaCl with 1000 µm WL to compare both bare and coated cathodic materials. Figure 15 shows a comparison of the bare SS316L and Ti-6Al-4V for the three fastener head geometries.

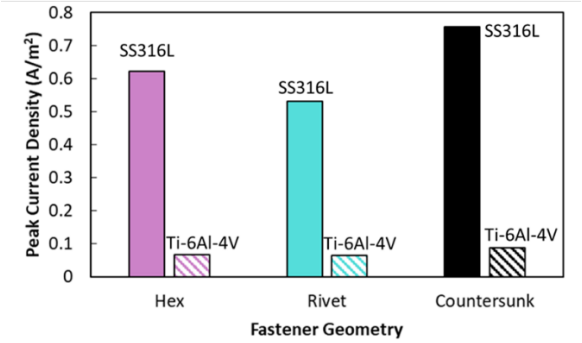

Figure 15. *Peak current density for AA7075 coupled with bare SS316L and Ti-64 in a 1000 µm WL of 0.6M NaCl.*

Across all three geometries, it can be seen that the stainless steel passes significantly more current to the aluminum alloy than the titanium fastener does. This was expected as SS316L has been observed to incites more corrosion damage than Ti-6Al-4V, but it served as a good baseline to compare the impact that the barrier coating may have on the reduction of the galvanic coupling current density.

The application of the sol gel barrier coating to the SS316L has a significant effect in the reduction of the predicted current density from the galvanic couple. A visual representation of this reduction is shown in the bar chart of Figure 16 for the SS316L and AA7075-T6 galvanic couple.

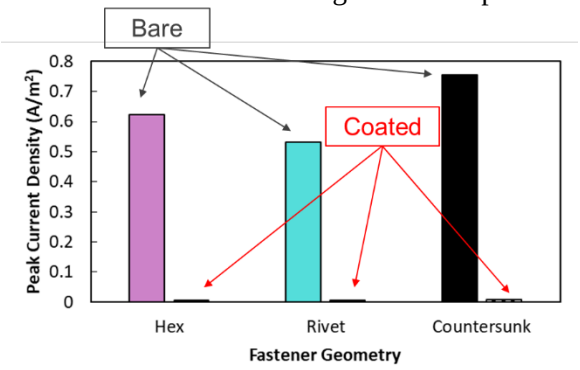

Figure 16. *Peak current density for AA7075 coupled with bare and coated SS316L in a 1000 µm WL of 0.6M NaCl.*

Based on the simulations from the SS316 bare and coated fasteners coupled with the AA7075 substrate, there is a huge advantage (approximately two orders of magnitude) to using this sol gel coating to reduce the cathodic kinetics and the driving force for galvanic corrosion. A similar, yet not so drastic effect takes place in the Ti-64 couple with 7075. The addition of the coating resulted in ~25x reduction in the peak current density. This is still a significant improvement in the reduction of the galvanic couple, but not nearly as large as the impact that the coating has on stainless steel.

In the four-fastener panel, several scenarios were studied including: bare fasteners, all coated fasteners, and one coated fastener. The galvanic couple used was AA7075 with bare and coated SS316L kinetics in 0.6M NaCl with a 1000 µm WL extending to the underside of the substrate plate around the fasteners. Figure 17 shows the modelled outputs for the current density distributions of these three scenarios.

The couple of bare stainless steel to the 7075-T6 resulted in current being concentrated down the fastener hole. This is due to the water layer extending beyond the aluminum substrate and coating the fastener on the underside of the panel. When the coating is applied to all of the fasteners, a reduction greater than 2 orders of magnitude is achieved in the peak current density, essentially removing the galvanic couple. When there is a bare fastener at the end of a galvanic panel. All of its current is passed locally under the fastener head and down the fastener hole. The other fastener holes are protected, although there is a very slight gradient in the current density as you move to fasteners across the panel from left to right.

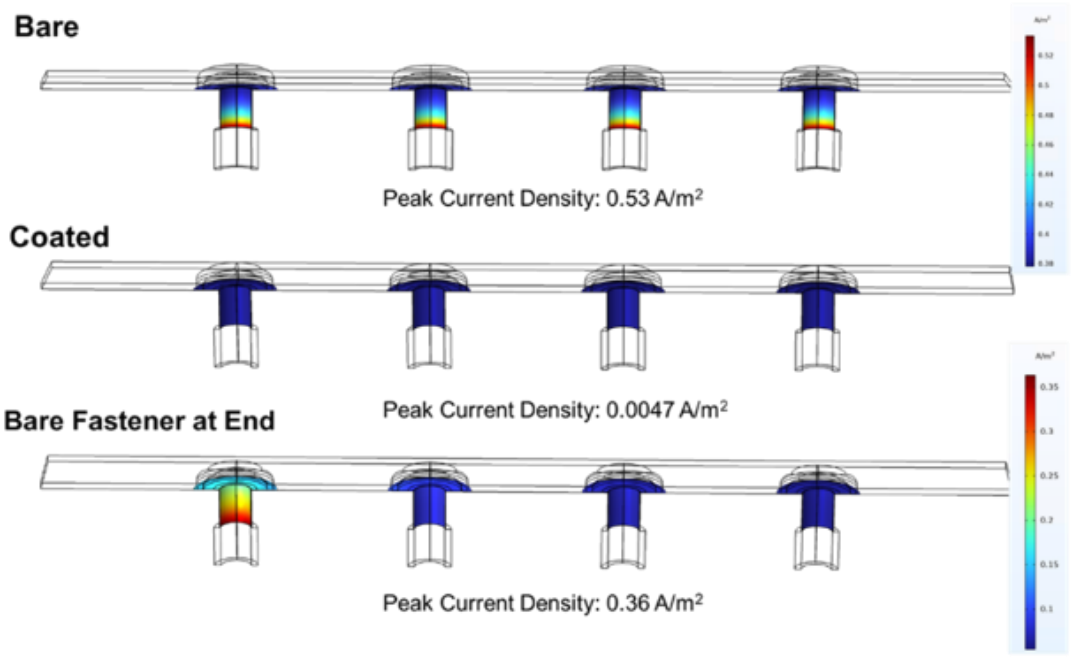

Figure 17. *Three modelling scenarios and the associated peak current densities for SS316L coupled with AA7075.*

While the current density is not quite as high for a single uncoated fastener, the current density down the fastener hole by the uncoated fastener is orders of magnitude higher than when all of the fasteners are coated. This suggests that even one uncoated fastener can have large implications on the acceleration of corrosion, albeit localized to a single fastener hole rather than across all of the bore holes in the panel. The position of the bare fastener either on the end or in one of the two middle positions did not significantly affect the output peak current density. This emphasizes the importance of reducing the cathode to anode ratio to reduce the galvanic corrosion damage and also shows how influential the coating of cathodic materials can be for improving corrosion resistance of multi-material aerospace structures.

Conclusions

- Anodic surface activation is significantly affected by the potentiostatic hold time and the solution concentration. An AA7075-T6 alloy will be undergo complete activation in 3M within 30 min at -256 $mV_{Ag/AgCl}$ while it will take 90 min for the same surface exposed in 0.6M NaCl.
- Increasing the scan rate during the PDP generation of the AAK increases the corrosion potential and current density up to a plateau at 100+ mV/s. This is due to the retention of Al^{3+} near the metal-solution interface by the reduction of the diffusion time allowed for these species.
- Scribe geometry does not significantly affect the peak current density and thus severity of corrosion predicted for the SS316L and AA7075 galvanic couple.
- The sol gel barrier coating has a dramatic effect on reducing galvanic current on both cathodes studied, nearly 100x for SS316L and 25x for Ti-6Al-4V.

Acknowledgements

Funding both from the Virginia Space Grant Consortium fellowship program and the Olsen Fellowship at the University of Virginia is greatly appreciated. The financial and technical support from A. Goff, F. Farelas, B. Clark, R. Marshall, V. Avance, and F. Friedersdorf of Luna Labs via Contracts 3632-AFR-2S/UVA and 3108-AFR-3S/UVA was influential in the completion of this

work. Any opinions, conclusions, and recommendations stated here are those of the author(s).

References

1. Marshall, R. S., Kelly, R. G., Goff, A. & Sprinkle, C. Galvanic corrosion between coated Al alloy plate and stainless steel fasteners, Part 1: FEM model development and validation. *Corrosion* **75**, 1461–1473 (2019).
2. Marshall, R. S., Goff, A., Sprinkle, C., Britos, A. & Kelly, R. G. Estimating the Throwing Power of SS316 when Coupled with AA7075 Through Finite Element Modeling. *Corrosion* **76**, 476–484 (2020).
3. Frankel, G. S. & McCreery, R. L. Inhibition of Al Alloy Corrosion by Chromates. *Electrochem. Soc. Interface* **10**, 34–38 (2001).
4. Feng, Z. & Frankel, G. S. Galvanic test panels for accelerated corrosion testing of coated al alloys: Part 2 - Measurement of galvanic interaction. *Corrosion* **70**, 95–106 (2014).
5. Palani, S., Hack, T., Deconinck, J. & Lohner, H. Validation of predictive model for galvanic corrosion under thin electrolyte layers: An application to aluminium 2024-CFRP material combination. *Corros. Sci.* **78**, 89–100 (2014).
6. Moraes, C. V, Santucci, R. J., Scully, J. R. & Kelly, R. G. Finite Element Modeling of Chemical and Electrochemical Protection Mechanisms Offered by Mg-Based Organic Coatings to AA2024-T351 Finite Element Modeling of Chemical and Electrochemical Protection Mechanisms Offered by Mg-Based Organic Coatings to. (2021) doi:10.1149/1945-7111/abfab8.
7. Liu, C. & Kelly, R. G. A review of the application of finite element method (FEM) to localized corrosion modeling. *Corrosion* **75**, 1285–1299 (2019).
8. Blohm, L. M., Liu, C. & Kelly, R. G. A Combined Experiment and Modeling Analysis of ASTM G85 WB Accelerated Corrosion Testing of Galvanically Coupled Sensitized AA5456-H116 and CDA 706 Cupronickel. *Corrosion* **77**, 1111–1122 (2021).
9. Mandel, M. & Krüger, L. FE-simulation of Galvanic Corrosion Susceptibility of two Rivet Joints Verified by Immersion Tests. *Mater. Today Proc.* **2**, S197–S204 (2015).
10. Murer, N., Missert, N. A. & Buchheit, R. G. Finite Element Modeling of the Galvanic Corrosion of Aluminum at Engineered Copper Particles. *J. Electrochem. Soc.* **159**, C265–C276 (2012).
11. Liu, C., Srinivasan, J. & Kelly, R. G. Editors' Choice—Electrolyte Film Thickness Effects on the Cathodic Current Availability in a Galvanic Couple. *J. Electrochem. Soc.* **164**, C845–C855 (2017).
12. Liu, C., Kubacki, G. W. & Kelly, R. G. Application of Laplace equation-based modeling into corrosion damage prediction for galvanic coupling between a zinc plate and stainless steel rods under a thin film electrolyte. *Corrosion* **75**, 465–473 (2019).
13. King, A. D., Electrochem, J. & Soc, C. Finite Element Analysis of the Galvanic Couple Current and Potential Distribution between Mg and 2024-T351 in a Mg Rich Primer Configuration Finite Element Analysis of the Galvanic Couple Current and Potential Distribution between Mg and 2024-T351 in a Mg. (2016) doi:10.1149/2.0171607jes.
14. Watanabe, Y. & Fujita, S. Development of Numerical Calculation Method of Formation of Corrosion Products in Galvanic Corrosion.
15. Snihirova, D. *et al.* Galvanic corrosion of Ti6Al4V -AA2024 joints in aircraft environment: Modelling and experimental validation. *Corros. Sci.* **157**, 70–78 (2019).
16. Liu, C., Khullar, P. & Kelly, R. G. Acceleration of the Cathodic Kinetics on Aluminum Alloys by Aluminum Ions. *J. Electrochem. Soc.* **166**, C153–C161 (2019).